Paramagnetic heavy-fermion ground state in single-crystalline UIr_2Zn_{20}

P. Swatek, M. Daszkiewicz, and D. Kaczorowski

Institute for Low Temperature and Structure Research, Polish Academy of Sciences, Post Office Box 1410, 50-950 Wrocław, Poland

(Received 14 December 2011; published 26 March 2012)

High-quality single crystals of UIr_2Zn_{20} were studied by means of x-ray diffraction, magnetic, electrical transport, and heat capacity measurements. In striking contrast with the literature data that classify the compound as an itinerant heavy-fermion ferromagnet with $T_C = 2.1$ K, no long-range magnetic ordering was found for the samples investigated down to 350 mK.

DOI: 10.1103/PhysRevB.85.094426 PACS number(s): 75.50.Lk, 75.50.Cc

I. INTRODUCTION

For more than half a century, uranium-based intermetallics have continuously attracted much scientific interest for their unusual physical properties. A point of controversy that despite many efforts has not been unambiguously solved until now is the nature of the $5f$ electronic states, which are responsible for magnetism in these materials. It is generally believed that in uranium intermetallics the $5f$ electrons are essentially itinerant, with the only fairly well-established exception being UPd_3.[1] Nevertheless, for several compounds, including heavy-fermion superconductors UPt_3 and UPd_2Al_3, one observed some features of the localized behavior, which accompany their predominantly itinerant electron characteristics.[2] Therefore, a theory of the dual character of the $5f$ electrons was formulated[3] which successfully accounts for the experimental data.

The apparent scarcity of uranium-based materials where the $5f$ electrons can be treated as purely localized makes the search for such systems very appealing. Recently, an important discovery in this field was reported in the literature,[4,5] namely that of the localized magnetism in the compounds UCo_2Zn_{20} and URh_2Zn_{20}. The two phases belong to a family of Zn-rich ternaries RT_2Zn_{20}, well known for their spectacular physical properties when R is a rare-earth atom (T stands for a d-electron transition metal).[6–9] The localized character of the $5f$ electrons in these compounds might be a consequence of expected negligible direct f-f magnetic exchange interactions (the shortest U-U distance is about 6 Å) and very weak f-ligand hybridization (U atoms are located in a nearly spherical polyhedron made by sixteen Zn atoms with closed outer electronic shells). Both phases, UCo_2Zn_{20} and URh_2Zn_{20}, were characterized in Refs. 4 and 5 as heavy-fermion compounds with paramagnetic ground states, and their properties were interpreted in terms of the Anderson impurity model in the single-ion Kondo limit. Moreover, an ionic-like electronic configuration of the uranium atoms was supported by the crystalline electric field effects recognized in the experimental data.

In contrast to the *localized* paramagnetic behavior established for UCo_2Zn_{20} and URh_2Zn_{20}, the isostructural compound UIr_2Zn_{20} was found by the same researchers to be an *itinerant* heavy-fermion system that orders ferromagnetically at 2.1 K.[4,10] Interestingly, the transition to the long-range ordered region was established to have a first-order character.

The intriguing findings of the entirely different nature of the $5f$ electronic states in the closely related compounds motivated us to undertake our own investigation on the UT_2Zn_{20} ternaries.[11] In the present paper we report our results obtained for high-quality single crystals of UIr_2Zn_{20}. Remarkably, they differ in several key aspects from those reported in the literature.

II. EXPERIMENTAL DETAILS

Single crystals of UIr_2Zn_{20} and $ThIr_2Zn_{20}$ were grown in zinc flux, following the recipe described in the literature.[12] Elemental purities were 99.9% for uranium and thorium (rods), 99.95% for iridium (powder), and 99.999% for zinc (droplets). The obtained crystals were well-developed cubes with dimensions up to 60 mm^3. They had metallic luster and were stable against air and moisture.

The quality of the crystals was checked by energy-dispersive x-ray analysis using a Phillips 515 scanning electron microscope equipped with an EDAX PV 9800 spectrometer. This examination revealed homogeneous single-phase materials with the composition equal within an experimental accuracy to the ideal 1:2:20 stoichiometry. No traces of any impurity elements were observed.

X-ray diffraction data were collected on a KUMA Diffraction KM-4 four-circle single-crystal diffractometer equipped with a charge-coupled device (CCD) detector using graphite-monochromatized MoK_α radiation ($\lambda = 0.71073$ Å). The raw data were treated with the CRYSALIS DATA REDUCTION PROGRAM (version 1.172.32.6),[13] taking into account an absorption correction. The intensities of the reflections were corrected for Lorentz and polarization effects. The crystal structures were solved by direct methods and refined by a full-matrix least-squares method using the SHELXL-97 program.[14]

Magnetic measurements were performed in the temperature range 1.8–300 K and in applied magnetic fields to 7 T using a Quantum Design MPMS-5 superconducting quantum interface device (SQUID) magnetometer. The specific heat and the electrical resistivity were studied over the temperature interval 0.35–300 K in external magnetic fields up to 9 T employing a Quantum Design PPMS-9 platform. Heat capacity measurements were made using an adiabatic heat-pulse technique. Electrical transport studies were carried out using a conventional four-point ac technique. The voltage and current leads (silver wires) were attached to bar-shaped specimens using silver epoxy glue.

TABLE I. Crystal data and structure refinement for single-crystalline UIr_2Zn_{20}.

Parameter	Value
Empirical formula	UIr_2Zn_{20}
Formula weight	1929.83 g/mol
Temperature	293(2) K
Wavelength	0.710 73 Å
Crystal system, space group	cubic, $Fd\bar{3}m$
Unit cell dimensions	$a = 14.2080(12)$ Å, $\alpha = 90^\circ$
	14.2080(12) Å, $\beta = 90^\circ$
	14.2080(12) Å, $\gamma = 90^\circ$
Unit cell volume	2868.1(4) Å^3
Z	8
Calculated density	8.938 Mg/m^3
Absorption coefficient	62.396 mm^{-1}
$F(000)$	6768
Crystal size	0.05 ×0.04 × 0.04 mm
θ range for data collection	$4.06^\circ \div 26.71^\circ$
Limiting indices	$-17 \leqslant h \leqslant 17$
	$-17 \leqslant k \leqslant 17$
	$-17 \leqslant l \leqslant 17$
Reflections collected / unique	9097 / 176 [R(int) = 0.1417]
Completeness to $\theta = 26.71$	99.4%
Absorption correction	numerical
Refinement method	full-matrix least-squares on F^2
Data / restraints / parameters	176 / 0 / 17
Goodness-of-fit on F^2	1.325
Final R indices [$I > 2\sigma(I)$]	$R_1 = 0.0381$, $wR_2 = 0.0922$
R indices (all data)	$R_1 = 0.0381$, $wR_2 = 0.0922$
Extinction coefficient	0.000 19(3)
Largest diff. peak and hole	1.863 eÅ^{-3} and −1.380 eÅ^{-3}

III. EXPERIMENTAL RESULTS AND DISCUSSION

A. Crystal structure

In accordance with the literature data,[10] our refinements of the crystal structure of UIr_2Zn_{20} from the single-crystal x-ray diffraction data yielded a cubic unit cell of the $CeCr_2Al_{20}$-type (space group $Fd\bar{3}m$, no. 227, $Z = 8$). Thus, the compound is isostructural with UCo_2Zn_{20} and URh_2Zn_{20} (Refs. 4 and 5) and the rare-earth-based ternaries RT_2Zn_{20} (R = Y, Nd, Sm, Gd-Lu).[6–9] Note the large number of atoms in the unit cell: 184. There are just one crystallographically inequivalent position for U atoms, one for Ir atoms, and three for Zn atoms. All these atoms have large coordination numbers [CN = 16, 12, 14, 12, and 12 for U, Ir, Zn(1), Zn(2), and Zn(3), respectively].

The main crystallographic data are collected in Table I. Table II gives the atomic positions and the isotropic thermal displacement parameters, Table III presents the anisotropic thermal displacement factors, while Table IV lists the shortest interatomic distances. It is worth noting that the refined lattice parameter $a = 14.2080(12)$ Å is somewhat larger than that reported before [$a = 14.1783(1)$ Å; Ref. 10]. Some discrepancies are observed also as regards the free positional parameters and the thermal displacement factors (compare Table 1 in Ref. 10), which may, however, partly result from the fact that the previous data were obtained for UIr_2Zn_{20} by means of powder neutron diffraction at $T = 0.6$ K (the final discrepancy factor in our x-ray study was $R = 3.81\%$, compared to $R = 13.04\%$ from the neutron data).

TABLE II. Atomic coordinates and equivalent isotropic displacement parameters for UIr_2Zn_{20}. U_{eq} is defined as one-third of the trace of the orthogonalized U_{ij} tensor.

Atom	x (×10^4)	y (×10^4)	z (×10^4)	U_{eq} (×10^{3}Å^2)
U	0.125	0.125	0.125	7(1)
Ir	0.5	0.5	0.5	7(1)
Zn(1)	0	0	0	18(1)
Zn(2)	0.4870(2)	0.125	0.125	12(1)
Zn(3)	0.0599(1)	0.0599(1)	0.3234(1)	13(1)

Figure 1 displays the cubic unit cell of UIr_2Zn_{20} that may be represented by packing of two kinds of Zn-based clusters around the U and Ir atoms, namely UZn_{16} and $IrZn_{12}$. The U atom is located inside a nearly perfect Frank-Kasper cubic polyhedron. The central atom has a cubic point symmetry $\bar{4}3m$. Twelve neighboring Zn atoms are located at a distance of 3.1074(19) Å, while four of them are at a distance of 3.0761(3) Å. These U-Zn bonds are distinctly larger than the sums of the relevant ionic, covalent, and atomic radii. In turn, the Ir atom is surrounded by six Zn atoms placed at a distance of 2.5184(3) Å (nearly equal to the sum of the Ir and Zn covalent radii) and six Zn atoms located at a distance of 2.7830(19) Å (somewhat larger than the sum of the relevant atomic radii). These ligands form a Frank-Kasper icosahedron around the Ir atom that occupies a site with trigonal point symmetry $\bar{3}m$. The three inequivalent Zn atoms in the unit cell of UIr_2Zn_{20} (see Table II) have trigonal point symmetries: $\bar{3}m$, m, and mm for Zn(1), Zn(2), and Zn(3), respectively. The coordination polyhedra of Zn(2) and Zn(3) are bicapped pentagonal prisms, whereas that of Zn(1) is a bicapped hexagonal prism.

Taking into account that in the unit cell of UIr_2Zn_{20} the U atoms are caged by the nonmagnetic Zn atoms (with closed electronic shell configuration $4s^23d^{10}$) and the shortest U-U spacing is there as large as 6.1522(9) Å, one may rule out any efficient direct as well as indirect (via f-d hybridization) magnetic exchange. Thus, one may expect that the compound remains paramagnetic down to the lowest temperatures. Moreover, the $5f$ electronic states in this compound may possibly bear localized character, like $4f$ electrons in its counterparts containing "normal" rare earths. In this context, the itinerant

TABLE III. Anisotropic displacement parameters (×10^3 Å^2) for UIr_2Zn_{20}. The anisotropic displacement factor exponent takes the form $-2\pi^2[h^2a^2U_{11} + \cdots + 2hkabU_{12}]$.

Atom	U_{11}	U_{22}	U_{33}	U_{23}	U_{13}	U_{12}
U	7(1)	7(1)	7(1)	0	0	0
Ir	7(1)	7(1)	7(1)	0(1)	0(1)	0(1)
Zn(1)	18(1)	18(1)	18(1)	−4(1)	−4(1)	−4(1)
Zn(2)	12(1)	12(1)	12(1)	−4(1)	0	0
Zn(3)	16(1)	16(1)	9(1)	0(1)	0(1)	−5(1)

TABLE IV. Interatomic distances (in Å) for UIr_2Zn_{20}.

Atoms	Length (Å)
U-4Zn(1)	3.0761(3)
U-12Zn(3)	3.1074(19)
Ir-6Zn(2)	2.5184(3)
Ir-6Zn(3)	2.7830(19)
Zn(1)-12 Zn(3)	3.0177(10)
Zn(1)-2U	3.0761(3)
Zn(2)-2Ir	2.5184(3)
Zn(2)-2Zn(3)	2.668(3)
Zn(2)-4Zn(2)	2.772(4)
Zn(2)-4Zn(3)	2.8079(17)
Zn(3)-1Zn(3)	2.616(2)
Zn(3)-1Zn(2)	2.668(3)
Zn(3)-2Zn(3)	2.678(3)
Zn(3)-1Ir	2.7830(19)
Zn(3)-2Zn(2)	2.8079(17)
Zn(3)-2Zn(3)	2.898(2)
Zn(3)-2Zn(1)	3.0177(10)
Zn(3)-1U	3.1074(19)

ferromagnetic ordering in UIr_2Zn_{20}, reported in Refs. 4 and 10, might appear most astonishing.

B. Magnetic properties

Figure 2 summarizes the magnetic data obtained for the prepared single crystal of UIr_2Zn_{20}. Above about 10 K, the magnetic susceptibility can be described in terms of a modified Curie-Weiss formula $\chi(T) = \chi_0 + \frac{C}{T-\Theta}$, where the parameter χ_0 accounts for a sum of Pauli contribution due to itinerant electrons and diamagnetic core contribution. The least-squares fit to the experimental data yields $\chi_0 = 1.12 \times 10^{-3}$ emu/mol, which is a typical magnitude of the Pauli paramagnetism in uranium-based heavy-fermion systems. The effective magnetic moment $\mu_{\rm eff} = \sqrt{8C} = 2.58\mu_B$ is notably smaller compared to the values expected within a localized Russell-Saunders coupling scenario for free U^{3+} and U^{4+} ions (3.58 and 3.62 μ_B, respectively). The derived paramagnetic Curie temperature Θ of about -2 K signals some weak antiferromagnetic correlations.

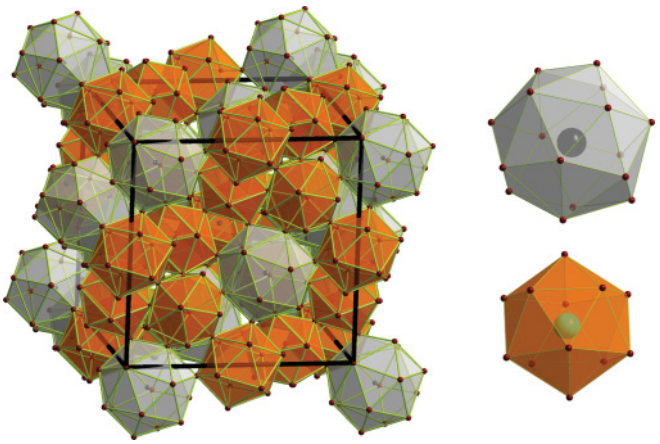

FIG. 1. (Color online) Crystal structure of UIr_2Zn_{20} shown as a packing of UZn_{16} (shaded in grey) and $IrZn_{12}$ (shaded in orange [dark gray]) clusters. The two polyhedra are presented on the right.

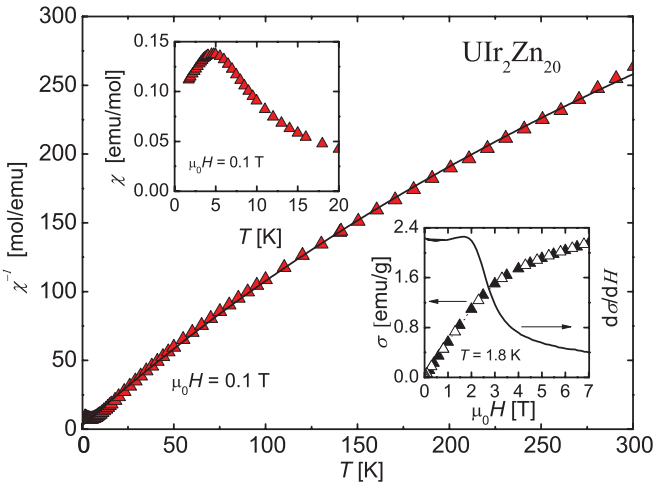

FIG. 2. (Color online) Temperature dependence of the inverse molar magnetic susceptibility of single-crystalline UIr_2Zn_{20} measured in a field of 0.1 T. The solid line is the modified Curie-Weiss fit described in the text. The upper inset shows the temperature dependence of the molar magnetic susceptibility below 20 K measured on heating (open symbols) and cooling (solid symbols) the specimen in $\mu_0 H = 0.1$ T. The lower inset presents the field variation of the magnetization in UIr_2Zn_{20} taken at 1.8 K with increasing (solid symbols) and decreasing (open symbols) magnetic field strength, as well as the field derivative of the magnetization data (solid curve).

As can be inferred from the upper inset of Fig. 2, the magnetic susceptibility of UIr_2Zn_{20} forms a maximum centered at 4.8 K. At first glimpse it may hint at antiferromagnetic ordering; however, more careful examination reveals that this feature is broad and quite symmetric in shape, unlike typical anomalies due to antiferromagnetic phase transitions. The observed singularity in $\chi(T)$ is entirely independent of magnetic history of the sample; that is, within an experimental error it is identical on heating and cooling in the same applied field. On the other hand, below about 25 K, the magnetic susceptibility is strongly dependent on the magnetic field strength. As can be inferred from Fig. 3, with increasing $\mu_0 H$ the maximum in $\chi(T)$ broadens and shifts to lower temperatures. As a result, in fields stronger than 2 T, the susceptibility of UIr_2Zn_{20} is a continuous function of the temperature down to the lowest temperatures studied. This finding clearly indicates magnetic origin of the observed anomaly.

The lower inset to Fig. 2 shows the magnetization isotherm measured for UIr_2Zn_{20} at 1.8 K, that is, much below the maximum in $\chi(T)$. Apparently, the magnetization is initially an almost linear function of the magnetic field strength and then shows some weak tendency toward saturation. No hysteresis effect is observed on decreasing field. The observed behavior of $\sigma(H)$ is in concert with that of $\chi(T)$, shown in Fig. 3, and consistently implies the paramagnetic (alternatively also antiferromagnetic) character of the electronic ground state in the crystal studied. This result is entirely different from the data previously reported for UIr_2Zn_{20}, which indicated

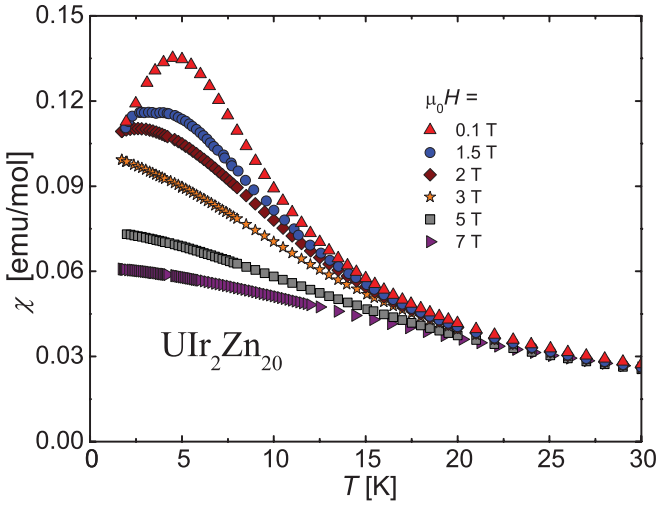

FIG. 3. (Color online) Low-temperature dependencies of the molar magnetic susceptibility of single-crystalline UIr_2Zn_{20} measured in a few different magnetic fields.

the ferromagnetic ordering below $T_C = 2.1$ K.[4,10] As can be inferred from the inset, the field derivative of the magnetization data exhibits a rapid drop with an inflection point near $\mu_0 H_m = 2.3$ T. Most importantly, this feature coincides with an anomaly in the electronic contribution to the specific heat (see below) and likely manifests a metamagnetic-like transition characteristic of heavy fermion systems.[15]

In contrast to the Curie-Weiss-like behavior of the magnetic susceptibility of the U-based compound, $\chi(T)$ of the $ThIr_2Zn_{20}$ single crystal (not shown) is diamagnetic, temperature independent, and very small (of the order of 2×10^{-4} emu/mol). This finding thus provides additional evidence that the χ_0 contribution to the magnetic susceptibility of UIr_2Zn_{20} arises due to the Pauli paramagnetism bearing the $5f$ electron character.

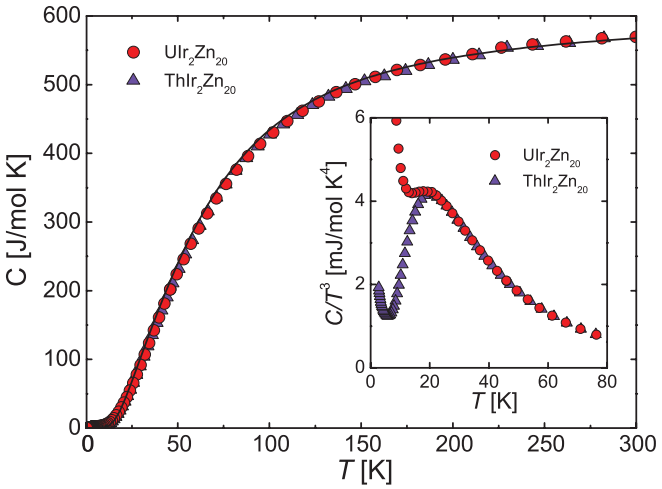

FIG. 4. (Color online) Temperature dependencies of the specific heat of single-crystalline UIr_2Zn_{20} and $ThIr_2Zn_{20}$. The solid line is the least-squares fit discussed in the text. The inset presents the low-temperature data of the two compounds plotted as C/T^3 versus T (for the sake of clarity the UIr_2Zn_{20} data below 8 K are omitted).

C. Heat capacity

Figure 4 shows the temperature variations of the specific heat of UIr_2Zn_{20} and $ThIr_2Zn_{20}$. At room temperature, the specific heat of both compounds achieves a value close to the Dulong-Petit limit for $r = 23$ atoms in the formula unit, that is, 560 J/(mol K). With decreasing temperature, $C(T)$ behaves in a nearly same manner, that is, the data overlap in an extended temperature interval down to about 20 K (see also the inset to Fig. 4). At lower temperatures, the specific heat of the U-based compound deviates from that of $ThIr_2Zn_{20}$, signaling the presence of significant magnetic contribution. As may be inferred from Fig. 5, $C/T(T)$ of UIr_2Zn_{20} forms a broad maximum near 3 K; however, no sharp peak is observed due to any magnetic phase transition. This result is in striking contrast with that reported in Refs. 4 and 10, yet in line with the magnetic data obtained for the present crystal.

At the lowest temperatures studied, the specific heat data of both compounds can be approximated by the classical formula $C/T = \gamma_0 + \beta T^2$ [see Fig. 5(a)], which accords with the simplest approach for the electronic and phonon contributions. For $ThIr_2Zn_{20}$, the proportionality $C/T \sim T^2$ is observed below about 6 K and the parameters derived from least-square fitting are $\gamma_0 = 13.1$ mJ/(mol K^2) and $\beta = 17.2 \times 10^{-6}$ mJ/(mol K^4). The latter value, via the expression $\beta = r\frac{12\pi^4}{5}\Theta_D^{-3}$, provides an estimate of 296 K for the Debye temperature Θ_D in $ThIr_2Zn_{20}$. Similar analysis of

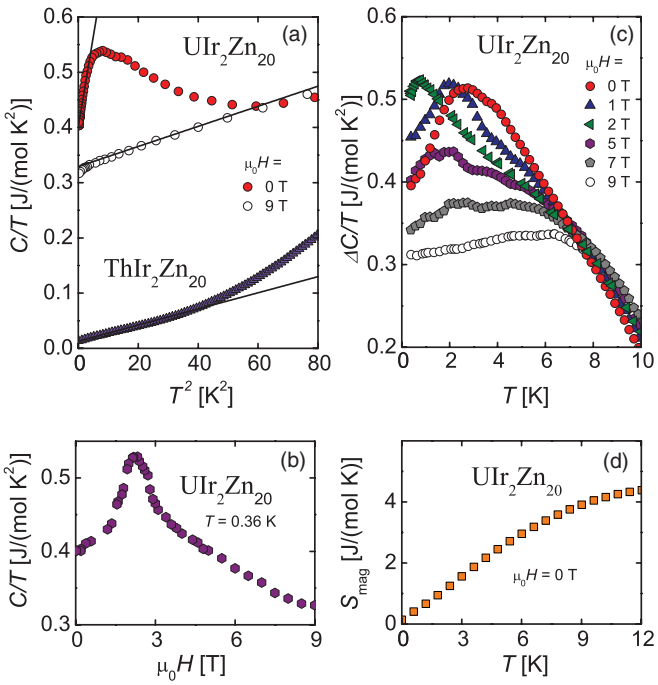

FIG. 5. (Color online) (a) Low-temperature specific heat data of single-crystalline UIr_2Zn_{20} and $ThIr_2Zn_{20}$ plotted as C/T versus T^2. For UIr_2Zn_{20}, the data measured in a magnetic field of 9 T are also shown (open circles). The solid straight lines are the least-squares fits discussed in the text. (b) Low-temperature variations of the excess specific heat of single-crystalline UIr_2Zn_{20}, presented as $\Delta C/T$, taken in a few different magnetic fields. (c) Magnetic field dependence of the specific heat in the form of C/T measured at 0.36 K. (d) Temperature dependence of the zero-field magnetic entropy.

the low-temperature data of UIr_2Zn_{20} is hampered by the presence of the maximum in C/T. Linearity in the C/T versus T^2 plot is observed only below 2 K and the extrapolated Sommerfeld coefficient is equal to 401 mJ/(mol K^2). However, upon applying a strong magnetic field, the maximum in C/T entirely disappears [see Fig. 5(a)] and the same fitting approach yields the parameters $\gamma_0 = 326$ mJ/(mol K^2) and $\Theta_D = 283$ K. Worth noting is that the derived values of the Debye temperature are nearly same in both compounds, as should be expected for isostructural systems. In turn, the distinct difference in the magnitude of the electronic contribution to the specific heat of $ThIr_2Zn_{20}$ and UIr_2Zn_{20} unambiguously demonstrates the heavy-fermion nature of the latter material.

The above analysis of the specific heat is expected to be valid only at temperatures much smaller than the Debye temperature ($T < \Theta_D/50$; Ref. 16). In order to get a more advanced description of $C(T)$ of the nonmagnetic $ThIr_2Zn_{20}$ compound in an extended temperature region, it was assumed that the phonon contribution can be represented in the form[17]

$$C_{\rm ph}(T) = \frac{1}{1-\alpha T}\left[\underbrace{9R\left(\frac{T}{\Theta_{\rm D}}\right)^3\int_0^{\Theta_D/T}\frac{x^4e^x}{(e^x-1)^2}dx}_{C_{\rm ph,D}} + \underbrace{\sum_i n_{\rm Ei}R\left(\frac{\Theta_{\rm Ei}}{T}\right)^2\frac{e^{\Theta_{\rm Ei}/T}}{(e^{\Theta_{\rm Ei}/T}-1)^2}}_{C_{\rm ph,E}}\right], \quad (1)$$

where α stands for the anharmonic coefficient, R is the gas constant, $C_{\rm ph,D}$ describes the Debye contribution of three acoustic modes (characterized by the Debye temperature Θ_D), and $C_{\rm ph,E}$ represents the Einstein specific heat calculated for i groups with $n_{\rm Ei}$ optical branches (characterized by the Einstein temperatures $\Theta_{\rm Ei}$). In order to avoid overparametrization, the numerical analysis of the of the experimental data of $ThIr_2Zn_{20}$ was made setting $\gamma_0 = 13.1$ mJ/(mol K^2) and $\Theta_D = 296$ K, as derived from the low-temperature fit. Moreover, one of the Einstein temperatures was fixed at $\Theta_{\rm E_1} = 110$ K, which was deduced from the position of a pronounced maximum seen in the plot C/T^3 versus T (cf. the inset in Fig. 4). With these assumptions, the entire $C(T)$ curve could be fairly satisfactorily described taking into account at least two other groups of optical branches (see the solid line in Fig. 4). Then, the least-squares fitting yielded the Einstein modes multiplicities $n_{\rm E1} = 33$, $n_{\rm E1} = 25$, and $n_{\rm E1} = 8$ and the Einstein temperatures $\Theta_{\rm E_2} = 232$ K and $\Theta_{\rm E_3} = 300$ K, while the anharmonic coefficient is $\alpha = 6 \times 10^{-5}$ 1/K. Here, it is worth emphasizing that despite the reasonable fitting of the experimental data in terms of Eq. (1), the results may not reflect the actual complexity of the lattice vibrations in $ThIr_2Zn_{20}$, and the presented approach gives at most only basic characteristics of the phonon spectra in this compound.

Figure 5(b) presents the excess heat capacity data of UIr_2Zn_{20} due to $5f$ electrons, obtained by subtracting $C(T)$ of $ThIr_2Zn_{20}$ from the total specific heat of the uranium compound. Apparently, the maximum in $\Delta C/T$ is sensitive to the magnetic field: it moves toward lower temperatures and becomes less distinct with increasing the external magnetic field strength, and in fields stronger than 3 T it cannot be discerned anymore. Instead, another broad hump develops in the applied fields that likely arises due to the Zeeman effect, as it gradually shifts to higher temperatures with rising field. As apparent from Fig. 5(c), the electronic contribution to the specific heat, estimated as the C/T ratio at $T = 0.36$ K, varies with the applied magnetic field is a highly anomalous manner. Initially, it rapidly increases from about 400 mJ/(mol K^2) in zero field up to a value of about 520 mJ/(mol K^2) observed near $\mu_0 H_m = 2.3$ T, and then slowly decays down to 320 mJ/(mol K^2) measured in 9 T. This behavior is reminiscent of that typical for metamagnetic heavy-fermion systems[15] and will be addressed in more detail in the next section.

The magnetic entropy calculated by integrating the zero-field $\Delta C/T$ data, $S_{\rm mag}(T) = \int \Delta C(T)/T dT$, attains at 12 K a value of 4.38 J/(mol K) [see Fig. 5(d)], which is significantly less than $R \ln 2 = 5.76$ J/(mol K), expected for a crystal-field split-doublet ground state with an effective spin quantum number $S = \frac{1}{2}$. Clearly, the obtained small magnetic entropy manifests an itinerant character of the $5f$ electronic states in UIr_2Zn_{20}.

D. Electrical transport properties

Figure 6 shows the temperature variation of the electrical resistivity of $ThIr_2Zn_{20}$. The resistivity measured at 300 K amounts to 24 $\mu\Omega$cm. With decreasing temperature it varies in a metallic manner, reaching at 0.35 K a residual value ρ_0 of about 4 $\mu\Omega$cm, which arises due to charge scattering on lattice defects. The residual resistivity ratio RRR $= \rho_{300\,\rm K}\rho_0 =$ 6 signals moderately high quality of the studied crystal. In the entire temperature range studied, $\rho(T)$ of $ThIr_2Zn_{20}$ can be described by means of the Bloch-Grüneisen-Mott (BGM) relation[18]:

$$\rho(T) = \rho_0 + \rho_{\rm BGM} = \rho_0 + 4R\Theta_{\rm R}\left(\frac{T}{\Theta_{\rm R}}\right)^5 \times \int_0^{\Theta_{\rm R}/T}\frac{x^5dx}{(e^x-1)(1-e^{-x})} - KT^3, \quad (2)$$

where the second term accounts for electron-phonon interactions and the third one describes the contribution due to Mott's s-d interband scattering. Least-squares fitting of the BGM formula to the experimental data in the entire temperature range studied yielded the values $\rho_0 = 4.1$ $\mu\Omega$ cm, $\Theta_{\rm R} = 144$ K, $R = 0.07$ $\mu\Omega$ cm K^{-1}, and $K = 3.5 \times 10^{-8}$ $\mu\Omega$ cm K^{-3}. The parameter $\Theta_{\rm R}$ is sometimes considered as an approximation of the Debye temperature. Clearly, such an estimation breaks

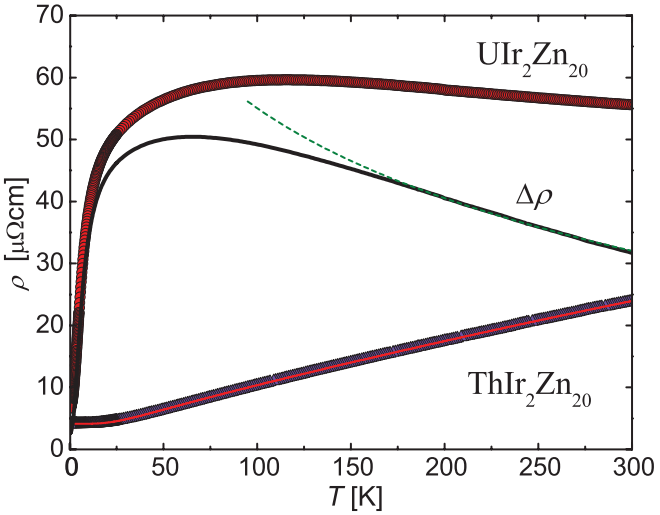

FIG. 6. (Color online) Temperature dependencies of the electrical resistivity of single-crystalline UIr_2Zn_{20} and $ThIr_2Zn_{20}$. The thick curve represents the sum of the residual and magnetic contributions to the resistivity of UIr_2Zn_{20}. The thin solid and dashed lines are the BGM and Kondo fits discussed in the text.

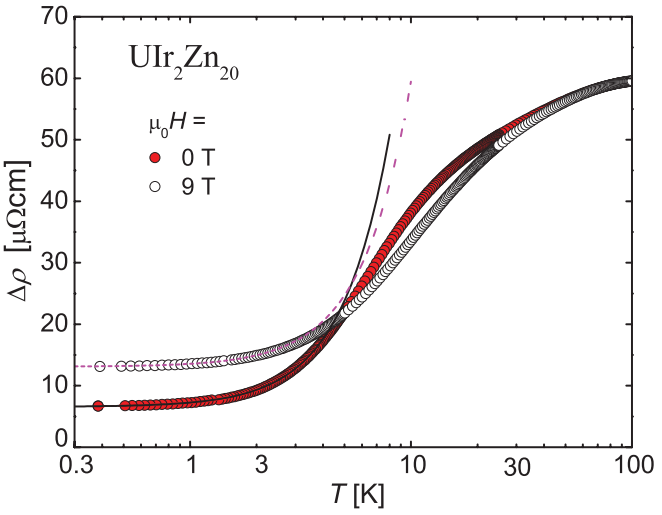

FIG. 7. (Color online) Low-temperature dependencies of the non-phonon electrical resistivity of single-crystalline UIr_2Zn_{20} measured in zero magnetic field and in a field of 9 T applied perpendicular to the electrical current. The solid lines are the Fermi liquid fits discussed in the text. Note a logarithmic temperature scale.

down for $ThIr_2Zn_{20}$, because Θ_D derived from the specific heat data is much larger than Θ_R.

The temperature dependence of the resistivity of single-crystalline UIr_2Zn_{20} is presented in Fig. 6. The overall shape of this curve is reminiscent of systems being dominated by spin fluctuations and spin-flip Kondo scattering. With lowering the temperature the resistivity first slightly increases, forms a broad maximum near 100 K, and finally drops rapidly below about 30 K. Except for the lowest temperatures (see below), this result is in qualitative agreement with the previous data;[10] however, the magnitude of ρ differs considerably. The resistivity of the measured crystal is about 56 $\mu\Omega$cm at room temperature, and it rises to 60 $\mu\Omega$cm at the maximum, while the reported data are 173 and 200 $\mu\Omega$cm, respectively. Similarly, the ρ_0 value of about 7 $\mu\Omega$cm in the present crystal is less than half that found for the specimen studied in Ref. 10. In turn, the present value of RRR = 8 is smaller than RRR = 12 reported before.

Assuming that the phonon contribution to the resistivity of UIr_2Zn_{20} can be properly approximated by that calculated for its Th-based counterpart, the contribution due to $5f$ electrons was derived. As may be inferred from Fig. 6, above about 160 K, the obtained resistivity data can be described by the function

$$\Delta\rho(T) = \rho_0 + \rho_{5f} = \left(\rho_0 + \rho_0^{\text{inf}}\right) + c_K \ln T, \qquad (3)$$

where the temperature-independent term comprises the residual resistivity ρ_0 and the spin-disorder resistivity ρ_0^{inf}, while the third term accounts for the Kondo scattering effect. Least-squares fitting the above formula to the experimental data yielded $\rho_0 + \rho_0^{\text{inf}} = 152$ $\mu\Omega$cm and -21 $\mu\Omega$cm.

Figure 7 illustrates the magnetic field dependence of the $\Delta\rho(T)$ variations derived for UIr_2Zn_{20} [the 9-T curve was obtained as described above, using $\rho(T)$ of $ThIr_2Zn_{20}$ taken in 9 T]. Above about 50 K, the resistivity is almost independent of the magnetic field strength. At lower temperatures, down to 5 K, the magnetic field suppresses the conduction electron scattering, whereas in the lowest temperature range studied the resistivity measured in the applied field is larger than that taken in zero field. Remarkably, the change in the character of the magnetic field influence on $\Delta\rho(T)$ occurs at a temperature that coincides with the position of the maximum in $\chi(T)$. Numerical analysis of the $\Delta\rho(T)$ curves indicated that both of them can be described below 5 K by the function $\Delta\rho(T) = \rho_0 + AT^2$. Remarkably, the proportionality $\rho \sim T^2$ is a characteristic feature of electron-electron interactions in a Fermi liquid. In UIr_2Zn_{20}, the parameters obtained for the zero-field curve are $\rho_0 = 6.6$ $\mu\Omega$cm and $A = 0.69$ $\mu\Omega$cm/K^2, while those derived from the 9-T data are $\rho_0 = 13.1$ $\mu\Omega$cm and $A = 0.46$ $\mu\Omega$cm/K^2. These results imply the Kadowaki-Woods ratio A/γ^2 of 4×10^{-6} and 5×10^{-6} $\mu\Omega$cm (mol K/mJ)^2 for the 0 and 9 T, respectively, which is fairly close to the universal value of 1.0×10^{-5} $\mu\Omega$cm (mol K/mJ)^2 expected for Fermi liquids.

The pronounced increase in the magnitude of the electrical resistivity of UIr_2Zn_{20}, which occurs at the lowest temperatures, is clearly evident from the transverse magnetoresistance isotherms presented in Fig. 8(a). At 0.4 K, the lowest temperature studied, the magnetoresistance MR $= [\rho(H) - \rho(0)]/\rho(0)$ rapidly increases with increasing field up to about 2.5 T and then shows only a minor rise up to $\mu_0 H = 9$ T, where MR achieves a value close to 100%. The observed distinct change in the behavior of MR corroborates the conjecture of the metamagnetic-like transition occurring at $\mu_0 H_m = 2.3$ T, deduced from the magnetization and specific heat data. As demonstrated in Fig. 8(a), in fields smaller than $\mu_0 H_m$, the magnetoresistance of UIr_2Zn_{20} is proportional to H^2. With increasing temperature, the value of the critical field decreases and the magnitude of the positive contribution to MR diminishes. In parallel, some negative contribution to the magnetoresistance becomes progressively more significant in strong magnetic fields. The interplay of these two opposite

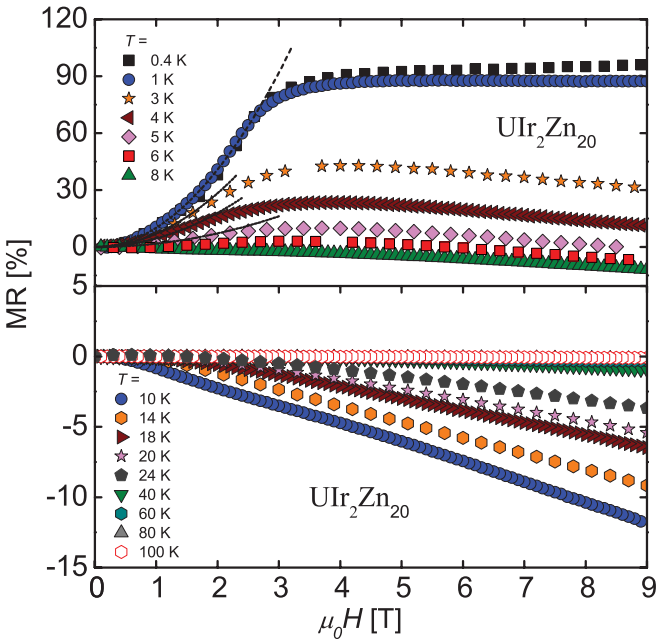

FIG. 8. (Color online) Magnetic field dependencies of the transverse magnetoresistance of single-crystalline UIr_2Zn20_20, taken at several different temperatures (a) below and (b) above 9 K. The dashed lines in panel (a) mark H^2 variations of the MR isotherms.

effects gives rise to the formation of broad maxima in MR(H), seen on all the isotherms taken at temperatures lower than 8 K. At higher temperatures [see Fig. 8(b)], MR is governed by the negative contribution in the entire magnetic field range studied, and its absolute magnitude rapidly decreases with increasing temperature. This finding is entirely in line with the Kondo character of UIr_2Zn_{20}, and the overall shape of the magnetoresistance isotherms is qualitatively consistent with the Bethe Ansatz result for MR in Kondo systems.[19]

IV. CONCLUSIONS

The compound UIr_2Zn_{20} crystallizes in the cubic $Fd\bar{3}m$ unit cell, like several other members of the UT_2Zn_{20} series with T = Fe, Ru, Co, Rh. In this structure type, the uranium atoms are located inside cages made of the zinc atoms, and their mutual interatomic distances are as large as about 6 Å. Because of those structural features any strong magnetic exchange interactions are unlikely. In line with such arguments, the high-quality single crystals of UIr_2Zn_{20} prepared in this study have been found paramagnetic down to the lowest temperatures studied (350 mK). The magnetic and thermodynamic data of UIr_2Zn_{20} described in this paper appear very similar to those reported for UCo_2Zn_{20} and URh_2Zn_{20} (Ref. 5). The characteristic features, common to all three compounds, are broad maxima in their low-temperature dependencies of the magnetic susceptibility and the specific heat. The authors of Ref. 5 suggested that these anomalies arise due to crystalline electric field potential acting on the well-localized $5f$ electrons. In our opinion, at low temperatures, the uranium $5f$ shell in the UT_2Zn_{20} ternaries is largely itinerant, as expected for heavy-fermion systems. Consequently, the maxima in $\chi(T)$ and $C(T)/T$ should be attributed to metamagnetic-like transitions, which have been evidenced for UIr_2Zn_{20} in the magnetic field variations of the magnetization and the electronic contribution to the specific heat at the critical field $\mu_0 H_m = 2.3$ T (see Figs. 2 and 5). Here, it is worthwhile recalling that very similar metamagnetic behavior is a characteristic property of archetypal paramagnetic heavy-fermion compounds like $CeRu_2Si_2$ (Ref. 20) and UPt_3 (Ref. 21). Furthermore, the metamagnetic transitions have recently been demonstrated for the Yb-based ternaries YbT_2Zn_{20}, where T = Co, Rh, and Ir,[22] which are isostructural counterparts to UIr_2Zn_{20}. For each of these heavy-fermion compounds, the maximum in $\chi(T)$ is observed at a characteristic temperature that approximately corresponds to the respective Kondo temperature. A similar estimate made for UIr_2Zn_{20} would imply $T_K \simeq 5$ K.

The paramagnetic ground state in UIr_2Zn_{20}, established in the present study, contrasts with the previous report on ferromagnetic ordering below 2.1 K.[4,10] In our opinion, this striking disagreement between the results of independent investigations may arise from tiny differences in the composition of the single crystals, synthesized from dissimilar initial molar ratios of the starting elements. Alternatively, the crystals investigated in the two laboratories might differ by the amount of atomic disorder in their crystallographic unit cell. The extreme sensitivity on structural effects of the magnetic behavior in the isostructural compound $TbFe_2Zn_{20}$ favors such a hypothesis.[23]

ACKNOWLEDGMENT

This work was supported financially by the National Science Centre (Poland) under Research Grant No. 2011/01/N/ST3/04488.

[1] Y. Baer, H. Ott, and K. Andres, Solid State Commun. **36**, 387 (1980).
[2] T. Takahashi, N. Sato, T. Yokoya, A. Chainani, T. Morimoto, and T. Komatsubara, J. Phys. Soc. Jpn. **65**, 156 (1996).
[3] G. Zwicknagl and P. Fulde, J. Phys. Condens. Matter **15**, S1911 (2003).
[4] E. Bauer, J. Thompson, J. Sarrao, and M. Hundley, J. Magn. Magn. Mater. **310**, 449 (2007).
[5] E. D. Bauer, C. Wang, V. R. Fanelli, J. M. Lawrence, E. A. Goremychkin, N. R. de Souza, F. Ronning, J. D. Thompson, A. V. Silhanek, V. Vildosola *et al.*, Phys. Rev. B **78**, 115120 (2008).
[6] M. S. Torikachvili, S. Jia, E. D. Mun, S. T. Hannahs, R. C. Black, W. K. Neils, D. Martien, S. L. Bud'ko, and P. C. Canfield, Proc. Natl. Acad. Sci. USA **104**, 9960 (2007).
[7] S. Jia, S. L. Bud'ko, G. D. Samolyuk, and P. C. Canfield, Nat. Phys. **3**, 334 (2007).
[8] S. Jia, N. Ni, G. D. Samolyuk, A. Safa-Sefat, K. Dennis, H. Ko, G. J. Miller, S. L. Bud'ko, and P. C. Canfield, Phys. Rev. B **77**, 104408 (2008).

[9]S. Jia, N. Ni, S. L. Bud'ko, and P. C. Canfield, Phys. Rev. B **80**, 104403 (2009).
[10]E. D. Bauer, A. D. Christianson, J. S. Gardner, V. A. Sidorov, J. D. Thompson, J. L. Sarrao, and M. F. Hundley, Phys. Rev. B **74**, 155118 (2006).
[11]P. Swatek and D. Kaczorowski, J. Phys. Soc. Jpn. **80**, SA106 (2011).
[12]P. C. Canfield and Z. Fisk, Philos. Mag. B **65**, 1117 (1992).
[13]M. Mayer, *CrysAlis Data Reduction Program* (Oxford Diffraction Ltd., Abingdon n. Oxford, 2006).
[14]G. M. Sheldrick, Acta Crystallogr. Sect. A **64**, 112 (2008).
[15]Y. Onuki, R. Settai, K. Sugiyama, T. Takeuchi, T. C. Kobayashi, Y. Haga, and E. Yamamoto, J. Phys. Soc. Jpn. **73**, 769 (2004).
[16]A. Tari, *The Specific Heat of Matter at Low Temperatures* (Imperial College Press, London, 2003).
[17]E. S. R. Gopal, *Specific Heats at Low Temperatures* (Plenum, New York, 1966).
[18]N. F. Mott and H. Jones, *The Theory of the Properties of Metals and Alloys* (Oxford University Press, London, 1958).
[19]P. Schlottmann, Z. Phys. B **51**, 223 (1983).
[20]P. Haen, J. Flouquet, F. Lapierre, and P. Lejay, J. Low Temp. Phys. **67**, 391 (1987).
[21]P. H. Frings and J. J. M. Franse, Phys. Rev. B **31**, 4355 (1985).
[22]Y. Hirose, M. Toda, S. Yoshiuchi, S. Yasui, K. Sugiyama, F. Honda, M. Hagiwara, K. Kindo, R. Settai, and Y. Onuki, J. Phys.: Conf. Ser. **273**, 012003 (2011).
[23]W. Tian, A. D. Christianson, J. L. Zarestky, S. Jia, S. L. Bud'ko, P. C. Canfield, P. M. B. Piccoli, and A. J. Schultz, Phys. Rev. B **81**, 144409 (2010).